nature materials

LETTERS

PUBLISHED ONLINE: 12 DECEMBER 2010 | DOI: 10.1038/NMAT2921

# Observation of empty liquids and equilibrium gels in a colloidal clay

Barbara Ruzicka[1]*, Emanuela Zaccarelli[2]*, Laura Zulian[3], Roberta Angelini[1], Michael Sztucki[4], Abdellatif Moussaïd[4], Theyencheri Narayanan[4] and Francesco Sciortino[2]

**The relevance of anisotropic interactions in colloidal systems has recently emerged in the context of the rational design of new soft materials[1]. Patchy colloids of different shapes, patterns and functionalities[2] are considered the new building blocks of a bottom-up approach toward the realization of self-assembled bulk materials with predefined properties[3–7]. The ability to tune the interaction anisotropy will make it possible to recreate molecular structures at the nano- and micro-scales (a case with tremendous technological applications), as well as to generate new unconventional phases, both ordered and disordered. Recent theoretical studies[8] suggest that the phase diagram of patchy colloids can be significantly altered by limiting the particle coordination number (that is, valence). New concepts such as empty liquids[8]—liquid states with vanishing density—and equilibrium gels[8–10]—arrested networks of bonded particles, which do not require an underlying phase separation to form[11]—have been formulated. Yet no experimental evidence of these predictions has been provided. Here we report the first observation of empty liquids and equilibrium gels in a complex colloidal clay, and support the experimental findings with numerical simulations.**

We investigate dilute suspensions of Laponite, an industrial synthetic clay made of nanometre-sized discotic platelets with inhomogeneous charge distribution and directional interactions. Similarly to other colloidal clays[12–14], Laponite has technological applications in cleansers, surface coatings, ceramic glazes, personal care and cosmetic products, including shampoos and sunscreens[15]. The anisotropy of the face–rim charge interactions, combined with the discotic shape of Laponite, produces a very rich phase diagram including disordered (gels and glasses) and ordered (nematic) phases, on varying colloidal volume fraction at fixed ionic strength[15–22]. At low concentrations the system ages very slowly up to a final non-ergodic state[19–21].

In this work we extend the observation time to timescales significantly longer than those previously studied and discover that, although samples seem to be arrested on the second timescale[19–21], a significant evolution takes place on the year timescale. Samples undergo an extremely slow, but clear, phase-separation process into clay-rich and clay-poor phases that are the colloidal analogue of gas–liquid phase separation. Spectacularly, the phase separation terminates at a finite but very low clay concentration, above which the samples remain in a homogeneous arrested state. At variance with respect to the structural transition previously observed for isotropic systems on a variation of density of depletants[23], this thermodynamic phase transition is driven by a change in colloid density (Laponite concentration). The observed features are instead strikingly similar to those predicted in simple models of patchy particles[8], suggesting that Laponite forms an (arrested) empty liquid at very low concentrations. Furthermore, in contrast to gels generated by depletion interactions[11,24] or from molecular glass-formers[25], where arrest occurs after the phase-separation process has generated high-density fluctuation regions, here phase separation takes place in a sample that is already a gel.

Figure 1a–c shows photographs of the temporal evolution of a low-concentration Laponite sample (weight concentration $C_w = 0.4\%$). The initially fluid suspension (waiting time $t_w = 0$) (Fig. 1a) progressively ages, forming a gel (the sample does not flow if turned upside down, as evident from Fig. 1b). The gelation time, as probed by dynamic light scattering, depends on clay concentration, and it is of the order of a few thousand hours for low-concentration samples[19]. Waiting significantly longer time (several years), the sample undergoes phase separation, creating a sharp interface between an upper transparent fluid and a lower opaque gel (Fig. 1c). Phase separation is observed for all samples with $C_w \lesssim 1.0\%$. Figure 1d shows a photograph of different concentration samples about three years after their preparation. The height of the colloid-rich part (indicated by the dashed lines in Fig. 1d) increases progressively with $C_w$, filling up the whole sample when $C_w \approx 1.0\%$. This value thus marks the threshold of the phase-separation region. We note also that the denser phase in all samples with $C_w < 1.0\%$ approaches $C_w^{gel} \approx 1.0\%$, that is, exactly the coexisting liquid density, as reported in Fig. 1e. This dense phase retains a memory of the separation process, remaining turbid even at very long times. The turbidity is due to the formation of large density fluctuations, generated during the phase-separation process, whose length scales are comparable to those of visible light. In contrast, higher-concentration samples ($C_w > 1.0\%$) do not show any phase separation and maintain their arrested and transparent character at all times (see the $C_w = 1.2\%$ sample in Fig. 1d). Furthermore, no macroscopic changes are observed in the entire concentration range in the following four years (seven years, around 60,000 h, in total).

To connect the absence of phase separation and turbidity in samples above the coexisting liquid density with the proposed equilibrium gel concept[8], as well as to characterize the structural evolution of the phase separation, we have investigated the evolution of the structure of Laponite samples for more than one year. Through small-angle X-ray scattering (SAXS) measurements, we have monitored the static structure factor $S^M(Q)$ at different waiting times, from the initial fluid phase up to the gel state (arrested according to light-scattering measurements) and during the initial stages of the phase-separation process. We have focused on two different concentrations, inside ($C_w = 0.8\%$) and outside

[1]CNR-IPCF and Dipartimento di Fisica, Università di Roma La Sapienza, Piazzale A. Moro 2, I-00185, Rome, Italy, [2]CNR-ISC and Dipartimento di Fisica, Università di Roma La Sapienza, Piazzale A. Moro 2, I-00185, Rome, Italy, [3]CNR-ISMAC via Bassini 15, 20133 Milan, Italy, [4]European Synchrotron Radiation Facility, B.P. 220 F-38043 Grenoble Cedex, France. *e-mail: barbara.ruzicka@roma1.infn.it; emanuela.zaccarelli@phys.uniroma1.it.

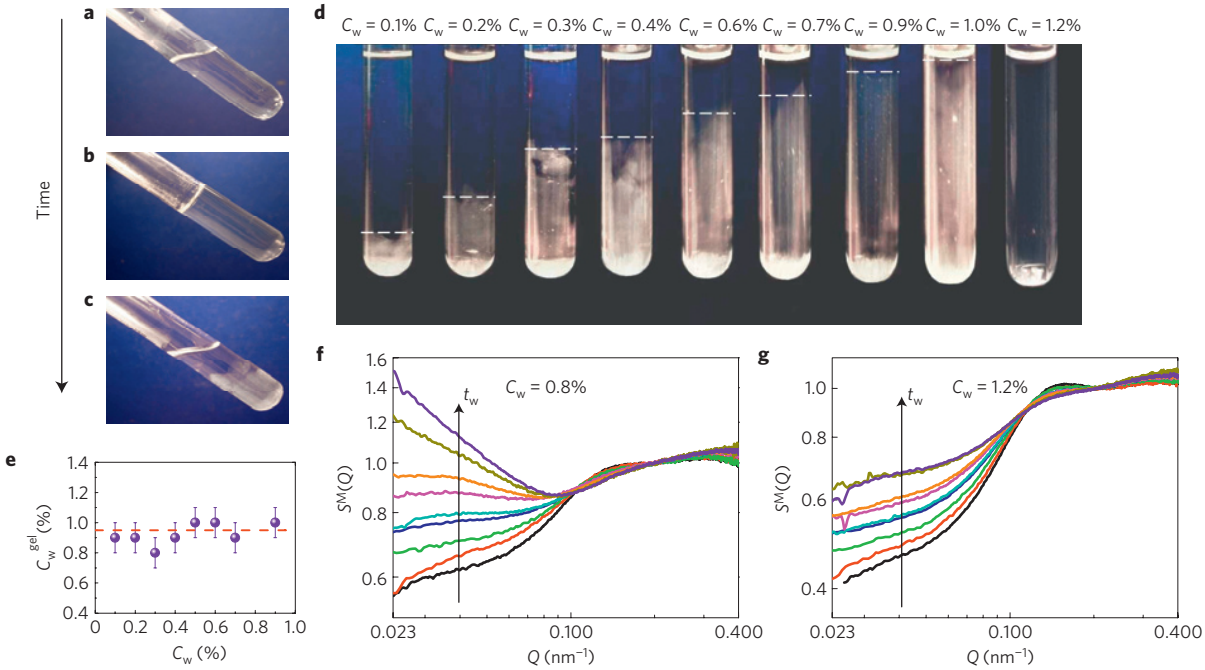


**Figure 1 | Experimental behaviour of diluted Laponite suspensions. a–c**, Photographs of a $C_w = 0.4\%$ sample in the initial fluid phase ($t_w = 0$) (**a**), in the gel state ($t_w \simeq 4{,}000$ h) (**b**) and in the phase-separated state ($t_w \approx 30{,}000$ h) (**c**). **d**, Photographs of samples in the concentration range $0.1 \leq C_w \leq 1.2\%$ at very long waiting times (about 30,000 h). All samples with $C_w \leq 1.0\%$ show clear evidence of two coexisting phases, separated by an interface whose height (dashed horizontal lines) increases progressively with $C_w$. **e**, Estimated concentration of the denser gel phase in the separated samples shown in **d**. **f**, Evolution of the measured $S^M(Q)$ with waiting time for a $C_w = 0.8\%$ sample (located inside the phase-separation region). **g**, Evolution of $S^M(Q)$ with waiting time for a $C_w = 1.2\%$ sample (located outside the phase-separation region). The curves in **f** and **g** are measured at increasing waiting times. From bottom to top, $t_w = 500$, 900, 1,600, 2,700, 3,400, 4,700, 6,000, 8,700 and 11,000 h.

($C_w = 1.2\%$) the phase-separation region. The measured $S^M(Q)$ are reported in Fig. 1f,g for different waiting times $t_w$. At short times $S^M(Q)$ shows a peak, induced by the overall electrostatic repulsion, at $Q \sim 0.15$ nm$^{-1}$, that is, a distance of $\approx$40 nm, which corresponds to platelets considerably far away from one another. With increasing $t_w$, this peak disappears in favour of a new peak emerging at $Q \gtrsim 0.4$ nm$^{-1}$, which corresponds to roughly contacting platelets in a T configuration ($\lesssim$15 nm). The shift of the main peak to higher $Q$ values is accompanied by a progressive increase of the intensity at small wavevectors, indicating the onset of aggregation for both concentrations. However, with the proceeding of the ageing dynamics, drastically different behaviour for the two samples is observed: whereas at $C_w = 0.8\%$ the small-$Q$ intensity continuously increases (Fig. 1f), at $C_w = 1.2\%$ the intensity saturates to a constant value at late times (Fig. 1g), as also shown in Supplementary Fig. S1.

The continuous increase of the small-$Q$ behaviour of $S^M(Q)$ for $C_w < 1.0\%$ signals the ongoing phase-separation process, also revealed by the sample turbidity. More interesting is the interrupted growth of $S^M(Q)$, accompanied by the formation of a macroscopic gel, which is observed for $C_w > 1.0\%$. As gelation must occur by way of a percolation transition, the system has organized itself into a spanning network. The saturation in the evolution of $S^M(Q)$, as time proceeds further, indicates that the system has reached its long-time equilibrium structure, that is, a stable network. The absence of further structural changes is consistent with the low effective valence of platelets, which at this point have formed most of their possible bonds. Owing to the low density of the system, the final gel state is rather non-compact, as signalled by the finite value of $S^M(Q)$ at small $Q$. During the entire aggregation process the system always remains transparent, confirming that fluctuations on a length scale comparable to the wavelength of light do not develop.

These results suggest that the samples outside the phase-separation region reach their equilibrium structure on the year timescale, whereas the samples inside the unstable region, despite their apparent gel state, slowly evolve toward complete phase separation. Thus, in Laponite gelation precedes, but does not pre-empt, phase separation.

To aid the interpretation of the previous results we introduce a primitive model of patchy discs, which aims to mimic the strong rim–face charge attraction and the tendency of Laponite clay to form open structures. Each platelet is schematized as a hard disc, following the work of ref. 26. To implement the rim–face linking (T bonds[27,28]) between different platelets, each disc is decorated with three sites on the rim and one at the centre of each face (five sites in total). Only face–rim bonds can form, and they are modelled with a short-range square-well attraction, ensuring that each site can be involved at most in one T bond. A representation of the model is provided in Fig. 2a and b.

We carry out Monte Carlo (MC) and Gibbs ensemble MC simulations to evaluate the gas–liquid coexistence region in the reduced density $\rho^*$ versus reduced temperature $T^*$ plane. Figure 2c shows the binodal line, that is, the locus of points separating homogeneous and phase-separated states, and the percolation line, defined as the line separating a finite-cluster fluid phase (Fig. 2d) from configurations characterized by the presence of a spanning infinite (transient) cluster. Figure 2e and f show snapshots of the simulated system at the percolation line. Consistent with previously studied patchy-sphere models[8], the gas–liquid coexistence region is confined in a narrow window of $T^*$ and $\rho^*$. Indeed, the coexisting liquid density, scaled by the close-packed value, occurs at significantly dilute conditions, $\rho^* \approx 0.114$. Hence, a wide region of densities exists above the coexisting liquid density where the system can be cooled down to very low $T$ without encountering phase separation, thus giving rise to an empty-liquid state[8]. Such a state consists of an extensively bonded percolating network (the equilibrium gel

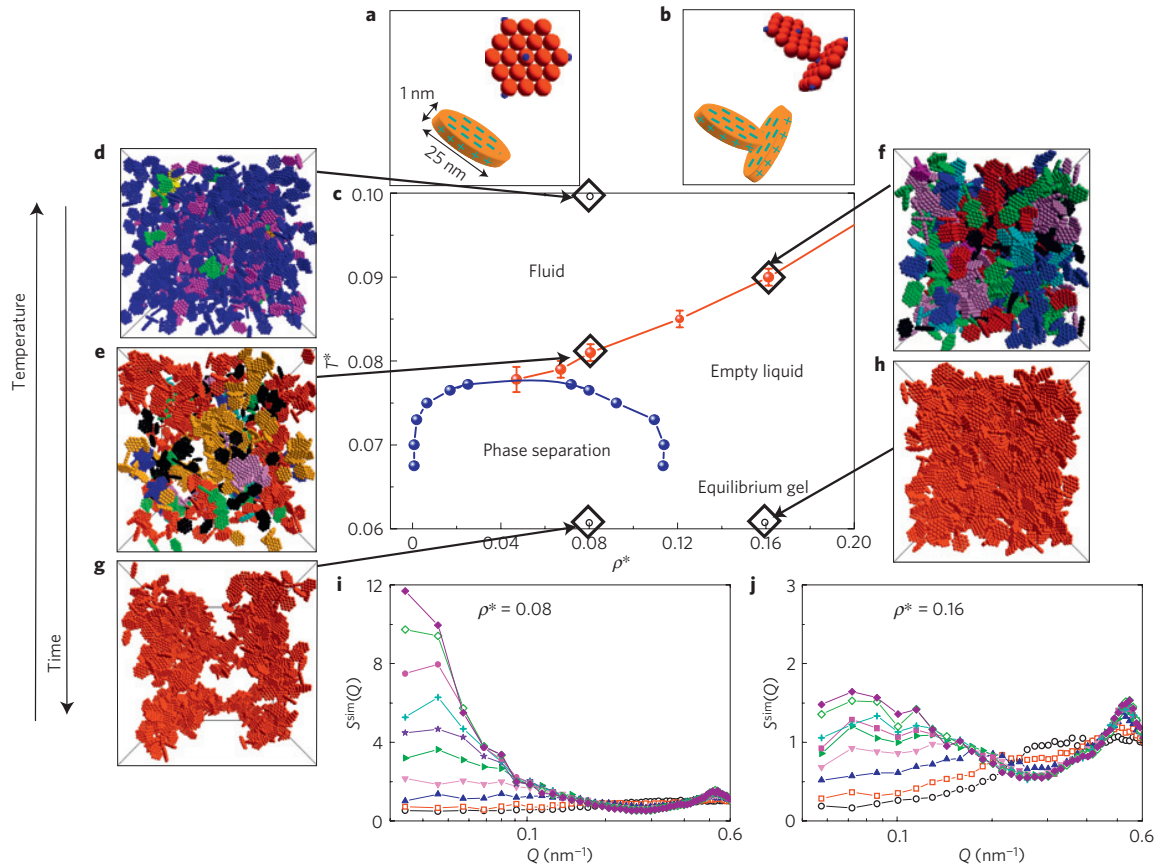


**Figure 2 | Behaviour of the patchy-particle model for Laponite discs. a**, Cartoon of a Laponite platelet and its schematization as a rigid disc composed by 19 sites (red spheres) with five attractive patches (blue spheres), three located on the rim and one at the centre of each face. **b**, Cartoon representing a T-bonded configuration for two interacting Laponite platelets and its realization in simulations. **c**, Numerical phase diagram: binodal (blue curve) and percolation locus (red curve) in the $\rho^*$–$T^*$ plane, where $\rho^*$ is the number density scaled by the close-packing density and $T^*$ is the thermal energy scaled by the strength of the bond (see Methods). **d**–**h**, Three-dimensional snapshots of MC simulations at different state points. Different colours correspond to different clusters, and the red colour is reserved for the percolating cluster. **d**, Equilibrium fluid phase at $T^* = 0.10$ and $\rho^* \simeq 0.08$. **e**,**f**, Equilibrium configuration at percolation for $\rho^* \simeq 0.08$ and 0.16. **g**,**h**, Final gel configurations at $T^* = 0.06$ inside ($\rho^* \simeq 0.08$) and outside ($\rho^* \simeq 0.16$) the phase-separation region. In these cases, platelets are connected into a single cluster (gel), which is clearly inhomogeneous (homogeneous) inside (outside) the binodal region. **i**,**j**, Evolution of the $S^{sim}(Q)$ after a quench at $T^* = 0.06$ for $\rho^* \simeq 0.08$ (inside the phase-separation region) and $\rho^* \simeq 0.16$ (outside the phase-separation region). Waiting times are $10^2, 1.2\times10^5, 5.7\times10^5, 1.6\times10^6, 3.6\times10^6, 6.1\times10^6, 10^7, 2.2\times10^7, 4.9\times10^7, 1.1\times10^8$ in MC steps.

state) that, at low $T$, restructures itself on a timescale that exceeds the observation time.

We also study the out-of-equilibrium dynamics of the model. To mimic the experimental protocol, we first equilibrate the system at high $T$ (corresponding to sample preparation) and then instantaneously quench it (corresponding to $t_w = 0$) to a sufficiently low $T$ that the bond energy is large as compared with the thermal energy, as in Laponite[16]. We propose to interpret the experimental behaviour as the low-$T$ limit of our model, connecting the increasing waiting time to a progressive temperature decrease in the numerical study[29]. Snapshots of the final configurations of the system after a quench inside and outside the phase-coexistence region are shown in Fig. 2g and h. Independently from the density of the quench, the final configuration is always characterized by a single spanning cluster incorporating all particles. The structure of such a cluster is highly inhomogeneous for quenches inside the coexistence region (Fig. 2g) and homogeneous for quenches in the empty liquid region (Fig. 2h). As at these low. $T$ values the bond lifetime becomes much longer than the simulation time, the bonded network is persistent, that is, the system forms a gel.

Figure 2i,j shows the static structure factors $S^{sim}(Q)$ calculated from MC configurations at several times (in MC steps, equivalent to $t_w$) following the quench, for two densities, respectively inside and outside the phase separation region. On increasing waiting time the scattered intensity increases in the region of the contact peak (T bonds, $Q \approx 0.5\,nm^{-1}$), the peak that monitors the aggregation kinetics, revealing the bond-formation process. The notable feature in $S^{sim}(Q)$ is the increase of the scattering at small wavevectors. As in the experimental data, two different scenarios occur at long times after preparation, respectively for samples inside (Fig. 2i) and outside (Fig. 2j) the unstable region. Although inside the phase-separation region $S^{sim}(Q)$ at small $Q$ increases indefinitely, outside this region the growth stops after a finite waiting time, showing no further evolution.

The zeroth-order model introduced here for describing Laponite at low densities condenses the electrostatic interactions between opposite charges into short-ranged attractive sites and ignores the overall repulsive electrostatic interactions, in the spirit of primitive models[30]. These simplifications lead to a different shape between experimental and numerical $S(Q)$ at short times—controlled in Laponite by the screened electrostatic interactions[31] (see Supplementary Information)—and in the absolute values of $S(Q)$ at small $Q$. However, the qualitative features shown by the model (Fig. 2i,j) coincide with those measured experimentally (Fig. 1f,g) both inside and outside the unstable region, pointing out that our model correctly captures the essential ingredients

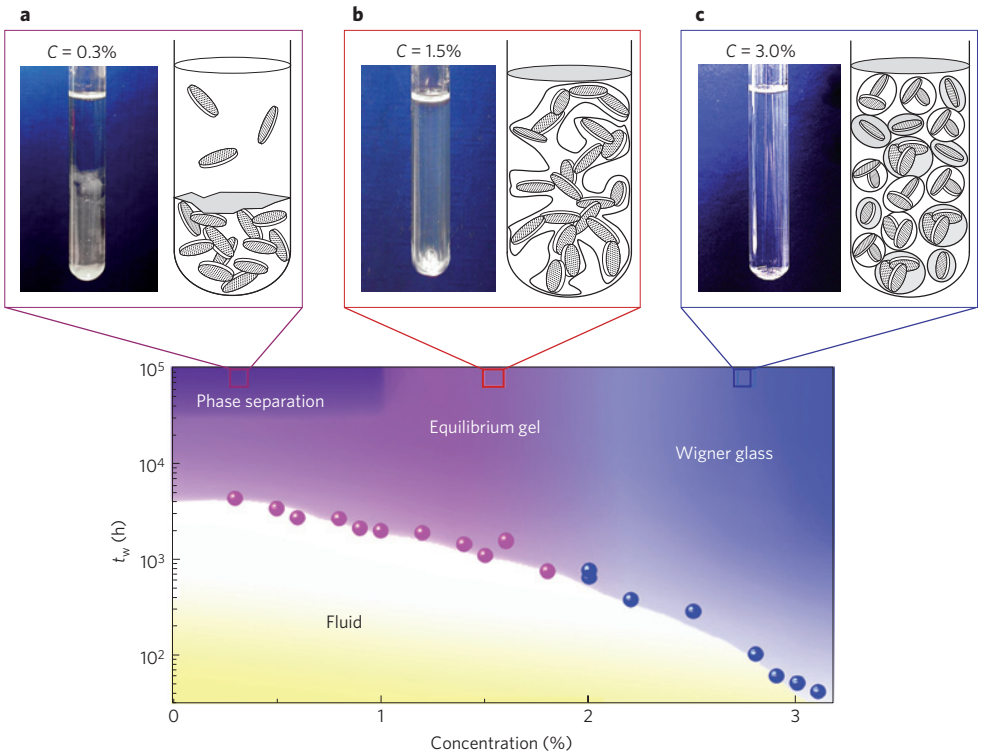


**Figure 3 | Phase diagram of diluted Laponite suspensions, in the waiting-time-versus-concentration plane, resulting from the combined experimental and numerical results.** Lower panel, Symbols correspond to experimental $t_w$ values required to observe non-ergodic behaviour by dynamic light scattering (ref. 19); boundaries inside coloured regions are guides to the eye. For long waiting times, three different regions are identified, whose representative macroscopic behaviour and a pictorial microscopic view are reported in **a**–**c**. **a**, Phase-separated sample with colloid-poor (upper part) and colloid-rich (lower part) regions for $C_w \leq 1.0\%$. **b**, Equilibrium gel for $1.0 < C_w < 2.0\%$, characterized by a spanning network of T-bonded discs. **c**, Wigner glass, expected for $2.0 \leq C_w \leq 3.0\%$ (ref. 31), where disconnected platelets are stabilized in a glass structure by the electrostatic repulsion, progressively hampering the formation of T bonds.

for describing the experimental behaviour. Most importantly, indefinite increase (saturation) in the growth of $S(Q)$ at small $Q$ is seen only inside (outside) the region where phase separation is observed, both in experiments and in simulations.

The present results suggest a new phase diagram of Laponite suspensions, summarized in Fig. 3, including the crossover taking place for $C_w \sim 2.0\%$ toward a Wigner glass[31]. At low concentrations, for $C_w \lesssim 1.0\%$, the system evolves through a sequence (Fig. 1a–c) of clustering (hours–days), gelation (months) and phase separation (years), from a sol to a homogeneous gel to a phase-separated sample in which only the dense phase is arrested. This progression with $t_w$ is strongly reminiscent of a constant-density path in the equilibrium phase diagram in which temperature is progressively decreased and the system evolves from a sol (Figs 1a, 2d) to a percolating structure (Figs 1b, 2e), finally encountering the phase-separation region (Figs 1c, 2g). Differently from the case of isotropic short-range attractive colloids[11], where a homogeneous fluid is driven by a spinodal decomposition into an arrested network, here the system first forms a gel and then the gel extremely slowly increases its local density to fulfil the search for a global-free-energy-minimum (phase-separated) state. These features are exactly those predicted to occur in patchy colloidal systems when the average valence is small[29], strongly supporting the view that the observed phase separation is a genuine effect of the directional interactions. The gel phase observed in Laponite above $C_w = 1.0\%$ can thus be interpreted as an arrested empty-liquid state, generated by the reduced valence, spontaneously arising from the combination of the platelet shape and the patchy distribution of opposite charges on the disc surface. The observed phase separation on the year timescale calls attention to the fact that the long-term stability of soft materials is controlled by the underlying phase diagram. Knowledge of thermodynamic properties is thus crucial in designing materials with desired properties. Our case study shows that a careful choice of the density (within the empty-liquid region) may provide materials that are extremely stable in the long term (gels that do not phase separate or age in the present case), because they are formed continuously from the liquid state, but finally reaching—through a very slow dynamics—their equilibrium configuration.

## Methods

**Laponite sample preparation.** Laponite RD suspensions were prepared in a glove box under $N_2$ flux and were always kept in a safe atmosphere to avoid sample degradation[32]. The powder, manufactured by Rockwood, was first dried in an oven at $T = 400\,^{\circ}C$ for 4 h and it was then dispersed in pure deionized water ($C_s \simeq 10^{-4}$ M), stirred vigorously for 30 min and filtered soon after through 0.45-μm-pore-size Millipore filters. Exactly the same protocol has been strictly followed for the preparation of each sample, a fundamental condition to obtain reliable and reproducible results[15]. At the end of this preparation process, Laponite forms a colloidal dispersion of charged disc-like particles, with a diameter of ∼25 nm and a thickness of ∼1 nm, with both negative charges on the faces and positive ones on the rims. The distinct rim and face charges induce a directional face–rim attraction, and a limited valence is realized by means of the extra electrostatic repulsion between like charges, which inhibits the formation of a large number of bonds per particle. The starting ageing time ($t_w = 0$) is defined as the time when the suspension is filtered.

The estimate of the denser-gel-phase concentration $C_w^{gel}$ in the phase-separated samples is provided by the ratio between the nominal concentration and the volume occupied by the dense phase, that is, ignoring the gas-phase concentration.

**Small-angle X-ray scattering.** SAXS measurements were made at the high-brilliance beamline (ID2) at the European Synchrotron Radiation Facility in Grenoble, France, using a 10 m pinhole SAXS instrument. The incident X-ray energy was fixed at 12.6 keV. The form factor $F(Q)$ was measured using

a flow-through capillary cell. SAXS data were normalized and the scattering background of water was subtracted. The measured structure factor has been obtained as $S^{M}(Q) = I(Q)/F(Q)$, where $I(Q)$ is the measured scattering intensity.

**Simulations.** Each platelet is modelled as a hard rigid disc composed of 19 sites on a hexagonal mesh, inspired by the work of ref. 26. Each site is a hard sphere of diameter $\sigma$, as schematically shown in Fig. 2a. A comparison with Laponite fixes $\sigma = 5$ nm. Each platelet is decorated with five sites, three located symmetrically on the rim and two on the two opposite faces of the central hard sphere. This primitive model highlights the anisotropic nature of the platelet–platelet interaction[26–28] but ignores the repulsive electrostatic barriers that control the timescale of the aggregation kinetics in Laponite (for a more detailed discussion, see Supplementary Information).

Site–site interactions (acting only between rim and face sites) are modelled as square-well interactions, with range $0.1197\,\sigma$ and depth $u_0 = 1$. The number of sites controls the effective valence of the model. As only rim–face bonds can be formed, the lowest-energy state is characterized by an average number of bonds per particle equal to four. The exact choice of the valence controls the location of the gas–liquid unstable region, but does not affect the topology of the phase diagram. Indeed, we have verified that, on variation of the number of rim charges, this topology is preserved, in full agreement with the case of spheres decorated by patches[8].

Reduced temperature $T^*$ is the thermal energy scaled by the strength of the bond, $T^* = k_B T/u_0$, where $k_B$ is the Boltzmann constant. Reduced density $\rho^*$ is defined as the number density $\rho = N/L^3$, where $N$ is the number of particles and $L$ the side of the cubic box, scaled by the close-packed density, corresponding to a hexagonal close packing of discs (which is space filling and equal to $\sqrt{(2)}/19\,\sigma^{-3}$). Gibbs ensemble MC simulations are carried out for a system of 250 platelets, which partition themselves into two boxes whose total volume is $66{,}603\,\sigma^3$, corresponding to an average number density $\rho^* \approx 0.05$. At the lowest studied $T$ this corresponds to roughly 235 particles in the liquid box and 15 particles in the gas box (of side $32\,\sigma$). On average, the code attempts one volume change every five particle-swap moves and 500 displacement moves. Each displacement move is composed of a simultaneous random translation of the particle centre (uniformly distributed between $\pm 0.05\,\sigma$) and a rotation (with an angle uniformly distributed between $\pm 0.1$ rad) around a random axis.

Standard MC simulations are carried out for a system of $N = 1{,}000$ platelets in the $NVT$ ensemble. An MC step is defined as $N$ attempted moves (defined as in the Gibbs ensemble MC method). Each state point is at first equilibrated at $T^* = 0.10$, and then quenched to $T^* = 0.06$, a temperature well below the critical one, where the system cannot reach equilibrium within the duration of the run. The waiting time is defined as the time of the quench. To reduce numerical noise at each waiting time, the observables of interest, such as the static structure factor $S(Q) = 1/N\langle|\rho_Q|^2\rangle$ with $\rho_Q = \sum_{j=1}^{N} \exp(iQ \cdot r_j)$, where $Q$ is the scattering wavevector and $r_j$ are the coordinates of the $j$th particle, are averaged over ten independent runs.

The use of a square-well potential to model the interactions makes it possible to unambiguously define two platelets as bonded when the pairwise interaction energy is $-u_0$. Clusters are identified as groups of bonded platelets. To test for percolation, the simulation box is duplicated in all directions, and the ability of the largest cluster to span the replicated system is controlled. If the cluster in the simulation box does not connect with its copy in the duplicated system, then the configuration is assumed to be non-percolating. The boundary between a percolating and a non-percolating state point is then defined as the probability of observing infinite clusters in 50% of the configurations.

Received 30 April 2010; accepted 9 November 2010; published online 12 December 2010

## References


1. Glotzer, S. C. & Solomon, M. J. Anisotropy of building blocks and their assembly into complex structures. *Nature Mater.* **8,** 557–562 (2007).
2. Pawar, A. B. & Kretzschmar, I. Fabrication, assembly, and application of patchy particles. *Macrom. Rapid Commun.* **31,** 150–168 (2010).
3. Manoharan, V. N., Elsesser, M. T. & Pine, D. J. Dense packing and symmetry in small clusters of microspheres. *Science* **301,** 483–487 (2003).
4. Zhang, G., Wang, D. & Möhwald, H. Decoration of microspheres with gold nanodots—giving colloidal spheres valences. *Angew. Chem. Int. Ed.* **44,** 1–5 (2005).
5. Mirkin, C. A., Letsinger, R. L., Mucic, R. C. & Storhoff, J. J. A DNA-based method for rationally assembling nanoparticles into macroscopic materials. *Nature* **382,** 607–609 (1996).
6. Kraft, D. J., Groenewold, J. & Kegel, W. K. Colloidal molecules with well-controlled bond angles. *Soft. Matter* **5,** 3823–3826 (2009).
7. Nykypanchuk, D., Maye, M. M., van der Lelie, D. & Gang, O. DNA-guided crystallization of colloidal nanoparticles. *Nature* **451,** 549–552 (2008).
8. Bianchi, E., Largo, J., Tartaglia, P., Zaccarelli, E. & Sciortino, F. Phase diagram of patchy colloids: Towards empty liquids. *Phys. Rev. Lett.* **97,** 168301–168305 (2006).
9. Zaccarelli, E. Colloidal gels: Equilibrium and non-equilibrium routes. *J. Phys. Condens. Matter* **19,** 323101–323151 (2007).
10. Saw, S., Ellegaard, N. L., Kob, W. & Sastry, S. Structural relaxation of a gel modeled by three body interactions. *Phys. Rev. Lett.* **103,** 248305–248309 (2009).
11. Lu, P. J. *et al.* Gelation of particles with short-range attraction. *Nature* **453,** 499–504 (2008).
12. Brown, A. B. D., Ferrero, C., Narayanan, T. & Rennie, A. R. Phase separation and structure in a concentrated colloidal dispersion of uniform plates. *Eur. Phys. J. B* **11,** 481–489 (1999).
13. Mourad, M. C. D. *et al.* Sol–gel transitions and liquid crystal phase transitions in concentrated aqueous suspensions of colloidal gibbsite platelets. *J. Phys. Chem. B* **113,** 11604–11613 (2009).
14. Shalkevich, A., Stradner, A., Bhat, S. K., Muller, F. & Schurtenberger, P. Cluster, glass, and gel formation and viscoelastic phase separation in aqueous clay suspensions. *Langmuir* **23,** 3570–3580 (2007).
15. Cummins, H. Z. Liquid, glass, gel: The phases of colloidal Laponite. *J. Non-Cryst. Solids* **353,** 3891–3905 (2007).
16. Mourchid, A., Delville, A., Lambard, J., Lecolier, E. & Levitz, P. Phase diagram of colloidal dispersions of anisotropic charged particles: Equilibrium properties, structure, and rheology of Laponite suspensions. *Langmuir* **11,** 1942–1950 (1995).
17. Mourchid, A., Lecolier, E., Van Damme, H. & Levitz, P. On viscoelastic, birefringent, and swelling properties of Laponite clay suspensions: revisited phase diagram. *Langmuir* **14,** 4718–4723 (1998).
18. Mongondry, P., Tassin, J. F. & Nicolai, T. Revised state diagram of Laponite dispersions. *J. Colloid Interface Sci.* **283,** 397–405 (2005).
19. Ruzicka, B., Zulian, L. & Ruocco, G. Routes to gelation in a clay suspension. *Phys. Rev. Lett.* **93,** 258301 (2004).
20. Ruzicka, B., Zulian, L. & Ruocco, G. More on the phase diagram of Laponite. *Langmuir* **22,** 1106–1111 (2006).
21. Jabbari-Farouji, S., Wegdam, G. H. & Bonn, D. Gels and glasses in a single system: Evidence for an intricate free-energy landscape of glassy materials. *Phys. Rev. Lett.* **99,** 065701–065704 (2007).
22. Shahin, A. & Joshi, Y. Irreversible aging dynamics and generic phase behavior of aqueous suspensions of Laponite. *Langmuir* **26,** 4219–4225 (2010).
23. Dibble, C. J., Kogan, M. & Solomon, M. J. Structural origins of dynamical heterogeneity in colloidal gels. *Phys. Rev. E* **77,** 050401–050404 (2008).
24. Buzzaccaro, S., Rusconi, R. & Piazza, R. Sticky hard spheres: Equation of state, phase diagram, and metastable gels. *Phys. Rev. Lett.* **99,** 098301–098304 (2007).
25. Sastry, S. Liquid limits: Glass transition and liquid–gas spinodal boundaries of metastable liquids. *Phys. Rev. Lett.* **85,** 590–593 (1999).
26. Kutter, S., Hansen, J-P., Sprik, M. & Boek, E. Structure and phase behavior of a model clay dispersion: A molecular-dynamics investigation. *J. Chem. Phys.* **112,** 311–322 (2000).
27. Dijkstra, M., Hansen, J-P. & Madden, P. A. Statistical model for the structure and gelation of smectite clay suspensions. *Phys. Rev. E* **55,** 3044–3053 (1997).
28. Odriozola, G., Romero-Bastida, M. & Guevara-Rodriguez, F. de J. Brownian dynamics simulations of Laponite colloid suspensions. *Phys. Rev. E* **70,** 021405–021420 (2004).
29. Sciortino, F. *et al.* A parameter-free description of the kinetics of formation of loop-less branched structures and gels. *Soft. Matter* **5,** 2571–2575 (2009).
30. Kolafa, J. & Nezbeda, I. Monte Carlo simulations on primitive models of water and methanol. *Mol. Phys.* **61,** 161–175 (1987).
31. Ruzicka, B. *et al.* Competing interactions in arrested states of colloidal clays. *Phys. Rev. Lett.* **104,** 085701–085704 (2010).
32. Thompson, D. W. & Butterworth, J. T. The nature of Laponite and its aqueous dispersions. *J. Colloid Interface Sci.* **151,** 236–243 (1991).


## Acknowledgements

B.R., L.Z. and R.A. thank G. Ruocco for his encouragement and advice during the course of this project. We thank C. De Michele for the code generating the snapshots of Fig. 2 and the European Synchrotron Radiation Facility for beamtime. E.Z. and F.S. acknowledge financial support from ERC-226207-PATCHYCOLLOIDS and ITN-234810-COMPLOIDS.

## Author contributions

B.R., L.Z. and R.A. carried out experiments. E.Z. and F.S. did the modelling and numerical simulations. M.S., A.M. and T.N. gave technical support and conceptual advice for the SAXS experiment. All authors discussed the results and implications and contributed to the writing of the manuscript.

## Additional information

The authors declare no competing financial interests. Supplementary information accompanies this paper on www.nature.com/naturematerials. Reprints and permissions information is available online at http://npg.nature.com/reprintsandpermissions. Correspondence and requests for materials should be addressed to B.R. or E.Z.